

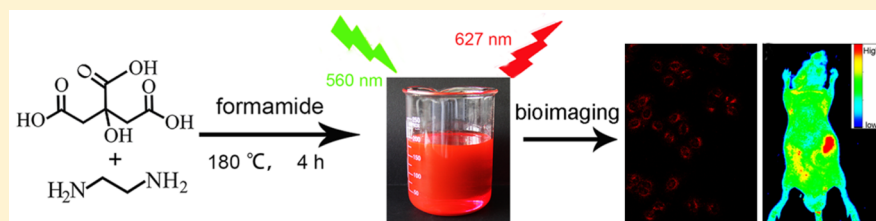
Highly Efficient Red-Emitting Carbon Dots with Gram-Scale Yield for Bioimaging

Hui Ding,[†] Ji-Shi Wei,[‡] Ning Zhong,[†] Qing-Yu Gao,[†] and Huan-Ming Xiong^{*,‡}

[†]College of Chemical Engineering, China University of Mining and Technology, Xuzhou 221008, Jiangsu, P. R. China

[‡]Department of Chemistry and Shanghai Key Laboratory of Molecular Catalysis and Innovative Materials, Fudan University, Shanghai 200433, P. R. China

S Supporting Information



ABSTRACT: Carbon dots (CDs) are a new class of photoluminescent (PL), biocompatible, environment-friendly, and low-cost carbon nanomaterials. Synthesis of highly efficient red-emitting carbon dots (R-CDs) on a gram scale is a great challenge at present, which heavily restricts the wide applications of CDs in the bioimaging field. Herein, R-CDs with a high quantum yield (QY) of 53% are produced on a gram scale by heating a formamide solution of citric acid and ethylenediamine. The as-prepared R-CDs have an average size of 4.1 nm and a nitrogen content of about 30%, with an excitation-independent emission at 627 nm. After detailed characterizations, such strong red fluorescence is ascribed to the contribution from the nitrogen- and oxygen-related surface states and the nitrogen-derived structures in the R-CD cores. Our R-CDs show good photostability and low cytotoxicity, and thus they are excellent red fluorescence probes for bioimaging both *in vitro* and *in vivo*.

1. INTRODUCTION

Carbon dots (CDs), as a rising star in photoluminescent nanomaterials, have aroused tremendous attention in the past decade.^{1–3} They have unique optical properties distinguished from the traditional quantum dots, facile synthetic routes with numerous cheap starting materials, better photostability than organic fluorescence probes, and extremely low toxicity among inorganic nanoparticles.^{4–6} Although thousands of precursors and hundreds of synthetic methods have been developed, most of the reported CDs emitted blue-green luminescence under ultraviolet (UV) light and their emission colors strictly depended on the excitation light wavelengths.^{7–9} In general, the yellow or red fluorescence of CDs was only observed under a green or yellow laser irradiation, and such excitation-dependent emission heavily hindered further applications of CDs in bioimaging. In addition, UV light irradiation is not suitable for bioimaging because it induces strong tissue autofluorescence to disturb the signals of CDs and damage the cells and tissues.^{10–12}

By far, only several research groups have reported long-wavelength emissive CDs. For example, Hu et al. first produced red luminescent CDs from complicated procedures, but the QY of their R-CDs was only 6%.¹³ Qu et al. reported orange emissive CDs with QY up to 46%, but the emission peak of their CDs did not locate at the red light region.¹⁴ Recently, Lin et al. synthesized R-CDs with QY of 16.2% in water for cell experiments, but the purification processes were time-

consuming.¹⁵ Our group prepared aqueous R-CDs with QY of 24% through a hydrothermal reaction and a careful chromatography separation, but only a small amount of R-CDs was finally obtained and the purification processes were also cumbersome.¹⁶ Therefore, it is still a challenge for chemists to produce highly luminescent R-CDs on a large scale in a facile route.

Herein, we report a simple and fast method to synthesize R-CDs on a gram scale with a PL peak at 627 nm and an absolute QY of 53%. Such a high QY value is outstanding for R-CDs at present, and the red fluorescence of our R-CDs can be seen clearly in the room light. Our R-CDs possess a much larger nitrogen content of 30% and a higher graphitization degree in comparison with other reported CDs using the similar raw materials. After detailed characterizations on the R-CDs and the NaBH₄ reduced R-CDs, we believe the surface states on CD surfaces, including the C=O and C=N functional groups, and those nitrogen-derived structures in CD cores are synergistically responsible for the intensive red fluorescence. Our R-CDs exhibit excitation-independent emission, good photostability, low cytotoxicity, and stable dispersity in water. They are successfully applied for bioimaging both *in vitro* and *in vivo* because the red fluorescence is able to penetrate animal bodies

Received: July 8, 2017

Revised: September 23, 2017

Published: October 17, 2017

Scheme 1. Synthetic Route of the R-CDs and the Product under Room Light

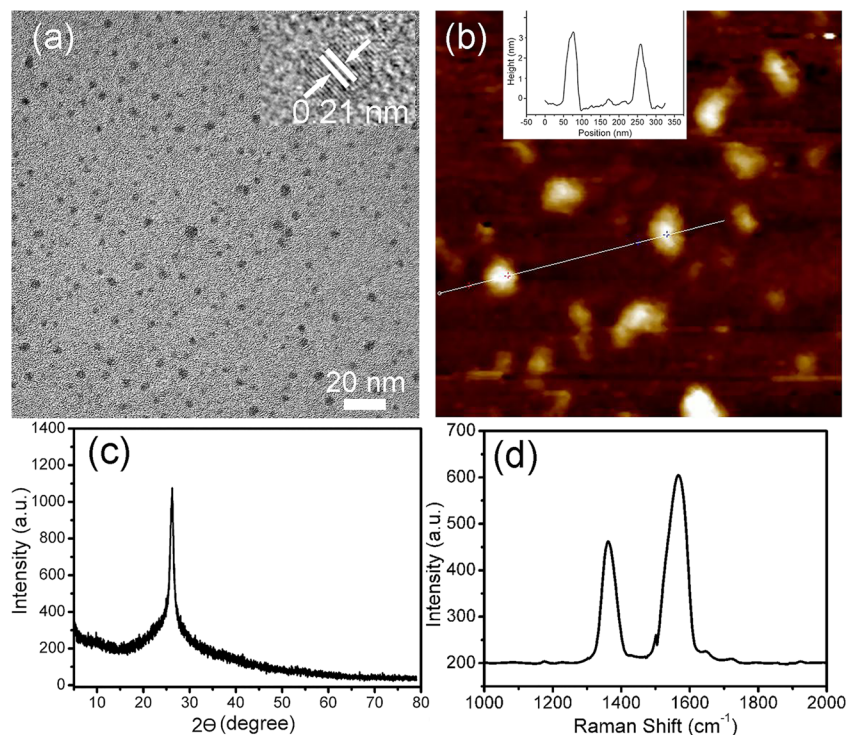
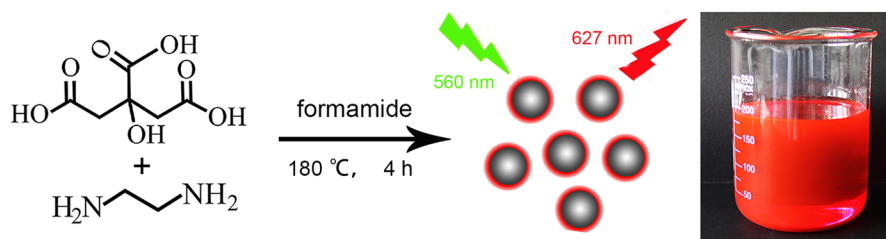


Figure 1. (a) TEM and HRTEM (inset) images of the R-CDs. (b) AFM image of the R-CDs and the (inset) corresponding height profile along the white line in (b). (c) XRD patterns and (d) Raman spectra of the R-CDs.

and overcome the interference of the autofluorescence of animal tissues.

2. EXPERIMENTAL SECTION

2.1. Materials. Citric acid, ethanediamine, formamide, ethanol, and acetone were from Sinopharm Chemical Reagent Co., China. 3-(4,5-Dimethylthiazol-2-yl)-2,5-diphenyltetrazolium bromide (MTT) was from Sigma-Aldrich. Dulbecco's modified Eagle's medium (DMEM, High Glucose), fetal bovine serum (FBS), and trypsin were from Gibco BRL (USA). All chemical reagents were used as received. Ultrapure water (Milli-Q water) was used throughout the experiments.

2.2. Sample Preparation. For synthesis of R-CDs, 1.2 g of citric acid and 2.1 mL of ethanediamine were dissolved in 80 mL of formamide to form a transparent solution. Then, the solution was transferred into a poly(*p*-phenol)-lined stainless steel autoclave for solvothermal reaction. After heating treatment at 180 °C for 4 h and cooling down to room temperature, the obtained mixture was filtered through filtration membrane (0.22 μm) to remove large particle residues. Subsequently, 200 mL of acetone was added to precipitate the solid R-CDs. Afterward, the precipitation was collected by centrifugation (10 000 rpm, 10 min) followed by washing with ethanol/acetone mixtures for several times and dried in a vacuum. Finally, nearly 1.0 g of dark powder was obtained.

For reduction of the as-prepared R-CDs, R-CDs powder (0.1 g) was dispersed into water (15 mL) followed by adding an excessive amount of NaBH₄, and the mixture was stirred at room temperature for 4 h.

The obtained solution was transferred into a dialysis bag (molecular weight cutoff 1000) for dialysis against deionized water for 1 day. For oxidation of the as-prepared R-CDs, R-CDs powder (0.1 g) was added into a HNO₃ aqueous solution (3 M, 15 mL) and refluxed for 12 h. Then, the as-obtained solution was neutralized with Na₂CO₃ followed by dialysis against water for 1 day.

2.3. Characterization. A Tecnai G2 F20 transmission electron microscope operating at 200 kV was utilized to obtain high-resolution transmission electron microscopy (TEM) images. The ultraviolet–visible (UV–vis) absorption spectra were measured on a PERSEE T10CS UV–vis spectrometer. The fluorescence spectra were recorded using an F-4600 spectrofluorometer. The FT-IR spectra were recorded on a VERTEX 80v spectrometer. The Raman spectra were recorded using a Senterra Raman spectrometer at an excitation wavelength of 785 nm. The X-ray photoelectron spectra were recorded using an ESCALAB 250Xi spectrometer (Thermo Fisher). The crystal structure was characterized by a Bruker D8 Advance X-ray diffractometer ($\lambda = 0.151\ 056\ \text{nm}$). The time-resolved fluorospectroscopy was performed using an FLS 920 spectrometer. The dynamic light scattering (DLS) spectra were recorded on a Malvern ZS-90 Zetasizer.

2.4. MTT Assays. HeLa cells were seeded into a 96-well cell culture plate in DMEM at a density of 5×10^4 cells/mL with 10% FBS and 5% CO₂ and incubated at 37 °C for 24 h. Afterward, the culture medium was replaced with 200 μL of DMEM containing the R-CDs at different doses, and the cells were cultured for another 48 h. Then, 20 μL of 5 mg/mL MTT solution was added to each cell well. The cells were

incubated for another 4 h, followed by the removal of the culture medium with MTT, and then 150 μL of DMSO was added to each well. The resulting mixture was shaken for 15 min at room temperature. The absorbance of MTT at 492 nm was measured using an automatic ELISA analyzer (SPR-960). Control experiments without R-CDs were also conducted. Each experiment was performed five times, and the averaged data were presented.

2.5. Cell Imaging. Cellular fluorescence images were recorded using an FV10i laser scanning confocal microscope. HeLa cells were seeded into 6-well culture plates at a density of 10^5 per well in DMEM containing 10% FBS and incubated at 37 $^\circ\text{C}$ in a 5% CO_2 incubator for 24 h. After the removal of the DMEM, a mixture of R-CDs (50 $\mu\text{g}/\text{mL}$) in DMEM was added to each well for 1 h of incubation. Finally, the cells were washed twice with phosphate buffer solutions to remove extracellular CDs and subsequently fixed with 4% paraformaldehyde.

2.6. Animal Imaging. The animal protocols of this study were approved to be appropriate and humane by the institutional animal care and use committee of the Chinese Academy of Sciences. Animal experiments were performed by strictly following the guidelines and regulations from the Laboratory Animal Centre of Chinese Academy of Sciences (Shanghai, China). In brief, a balb/c nude mouse was subcutaneously injected with 50 μL of the R-CDs aqueous solution (1 mg/mL) at the injection site after being anesthetized by intraperitoneal injection of 1% pentobarbital. The FL images were taken under an excitation light of 535 nm and an emission filter of 600 nm. The animal fluorescence imaging was conducted using a Bruker *in vivo* imaging system, and the exposure time was 1.0 s for all fluorescence images.

2.7. QY Measurement. The quantum yield was tested using an integrating sphere attached to an F-4600 spectrofluorometer. At first, the R-CDs formamide solution was diluted to an absorption intensity of below 0.1 at the optimal excitation wavelength of 561 nm. Subsequently, this solution was added into a fluorescence cuvette, placed in the integrating sphere and excited with 561 nm monochromatic light. The fluorescence spectra were collected in the ranges 551–571 and 450–800 nm, respectively. Meanwhile, the same fluorescence spectra for pure formamide were also recorded under identical conditions. Finally, the QYs were calculated using fluorescence software based on the PL spectra of both the sample and the formamide. Each experiment was conducted by three times in parallel to obtain the averaged QY value.

3. RESULTS AND DISCUSSION

Experimentally, the R-CDs were synthesized solvothermally at 180 $^\circ\text{C}$ for 24 h (Scheme 1), followed by precipitation and washing for several times, and nearly 1.0 g of solid-state R-CDs powder was obtained finally (Figure S1). The as-obtained R-CDs were redispersed in formamide for optical characterizations and in water for biological experiments. When the R-CDs were redispersed in formamide, the solution shows bright red luminescence under daylight, suggesting their high PL efficiency and intense absorption in the visible region.

The TEM image in Figure 1a and the statistical result in Figure S2 show the R-CDs are monodispersed nanoparticles with an average diameter of about 4.1 nm. The high-resolution TEM image in the inset illustrates that the R-CDs have well-resolved lattice fringes with a spacing of 0.21 nm, attributed to the (100) in-plane lattice spacing of graphene.^{17,18} The atomic force microscopy (AFM) image in Figure 1b shows a thickness of about 3 nm for R-CDs, corresponding to about 5–6 graphene layers.¹⁹ The X-ray diffraction (XRD) pattern of the samples (Figure 1c) has an evident peak centered at around 26° for its (002) planes,²⁰ suggesting that the R-CDs consist of graphene-like structures, which is in agreement with the TEM and AFM results. According to the Debye–Scherrer formula,²¹ the average crystalline size of the R-CDs is calculated to be 2.6 nm, which is smaller than that observed by TEM. Such a

difference implies that the each R-CD nanoparticle consists of amorphous shells. In the Raman spectrum (Figure 1d), two bands at 1361 cm^{-1} (D band) and 1566 cm^{-1} (G band) are observed. The D band is ascribed to the disorder or defects, while the G band is from the sp^2 carbon networks in the graphitized structure.^{22–24} The intensity ratio between D band and G band is 0.77, suggesting a high degree of graphitization.

The FT-IR spectra in Figure 2 illustrate that the R-CDs samples possess abundant hydrophilic groups, such as O–H at

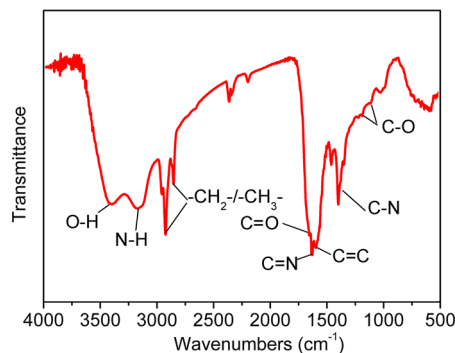


Figure 2. FT-IR spectra of the R-CDs.

3410 cm^{-1} , N–H at 3161 cm^{-1} , C=O at 1665 cm^{-1} , and C–O at 1283 cm^{-1} , thereby guaranteeing the excellent solubility of R-CDs in water.^{25,26} Moreover, the FT-IR bands at 1612, 1591, and 1457 cm^{-1} correspond to the C=N, C=C, and C–N stretching vibrations, respectively, implying the formation of polyaromatic structures in the CDs cores.^{27,28} The wide XPS spectrum in Figure 3a shows three typical peaks at 285, 400, and 531 eV, respectively, suggesting that the R-CDs samples are composed of C, N, and O elements.²⁹ Remarkably, in comparison with other previously reported CDs synthesized from the same recipes,^{20,30} our R-CDs have a much higher nitrogen content of 30% (Table S1), suggesting that amide in formamide can react with carboxyl groups of citric acids to form pyrrolic N species or pyridinic N species through the dehydrolysis reaction. In the high-resolution XPS spectra, the C 1s band (Figure 3b) can be deconvoluted into four peaks of C–C/C=C at 284.4 eV, C–N at 285.7 eV, C–O at 286.5 eV, and C=O/C=N at 287.8 eV.³¹ The N 1s spectrum (Figure 3c) displays three peaks at 399.5, 400.5, and 401.5 eV, attributed to pyridinic C–N–C, pyrrolic C₂–N–H, and graphitic N–C₃, respectively.³² The O 1s band (Figure 3d) contains two peaks at 531.6 and 532.9 eV for C=O and C–O, respectively.³³ The above data and analyses confirm that R-CDs consist of large π -conjugated domains in their cores and amorphous regions on their surfaces, and a large amount of nitrogen atoms is doped into the R-CDs samples.

The optical properties of the R-CDs were investigated and are shown in Figures 4a and 4b. The UV–vis absorption spectrum displays a broad absorption across the entire visible region with a main peak at about 564 nm, which could be originated from $n \rightarrow \pi^*$ transition of aromatic systems with many C–N/C=N or C–O/C=O structures.^{15,34} The PL spectrum of the R-CDs exhibits an outstanding excitation-independent PL behavior with the maximum emission peak at 627 nm. The PL excitation spectrum of the R-CDs is well overlapped with the absorption spectra in the long-wavelength region, indicating that nitrogen- and oxygen-related surface structures and states contribute to the intense red emission.

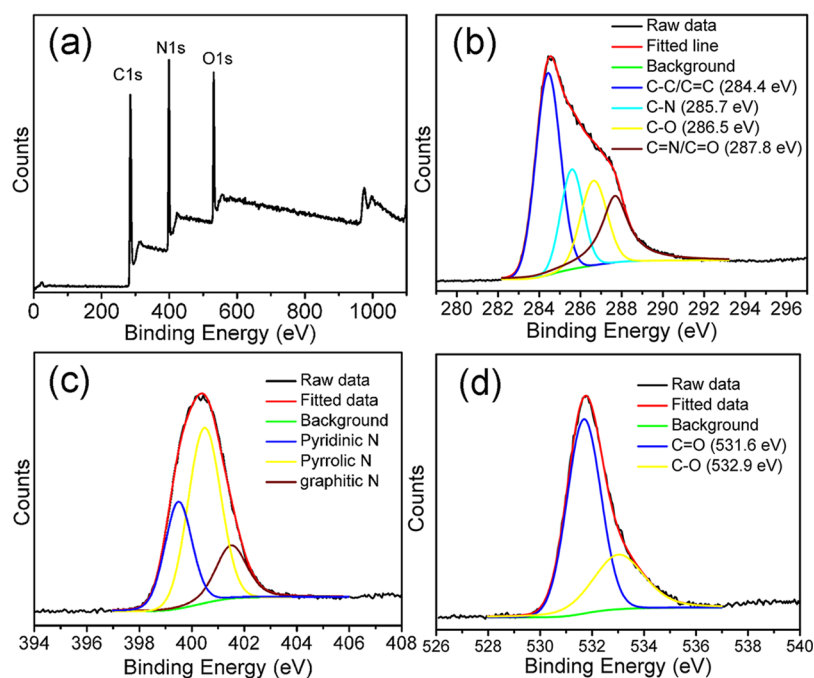


Figure 3. XPS spectra of the as-obtained R-CDs: (a) the wide spectra and high-resolution spectra of (b) C 1s, (c) N 1s, and (d) O 1s.

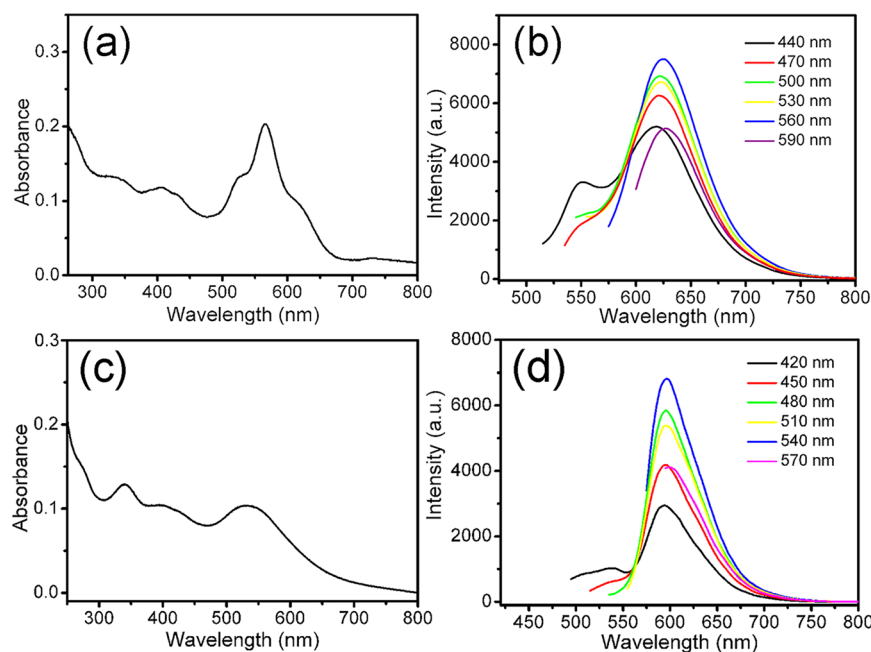


Figure 4. UV-vis absorption spectra of (a) the R-CDs and (c) the NaBH_4 -reduced R-CDs. PL emission spectra of (b) the R-CDs and (d) the NaBH_4 -reduced R-CDs excited by different wavelengths of light. All samples are dissolved in formamide.

The absolute QY of R-CDs is determined to be 53% using an integrating sphere under the optimal excitation light of 561 nm (Figure S3). The PL decay curves of the R-CDs (Figure 5) are fitted by a dual-exponential formula with an average lifetime of 3.2 ns (Table S1), which is close to those of other reported CDs and indicates the strong coupling between the surface states and the intrinsic states.^{35–37} Obviously, our R-CDs exhibit distinctive optical properties from those previously reported highly blue luminescent CDs (B-CDs) produced by hydrothermally treating citric acid and ethylenediamine in water.^{20,38,39}

To date, many mechanisms have been proposed to explain the PL origins of CDs, including the quantum size effects,^{14,40} and the intrinsic states in carbon cores⁴¹ or the surface states controlled luminescence.¹⁶ In the present work, we believe nitrogen- and oxygen-related surface states and nitrogen-derived structures in carbon cores are responsible synergistically for the intense red emission of the R-CDs because our R-CDs have the similar particle sizes and size distributions but a higher nitrogen content in comparison with those previously reported blue-emitting CDs.^{42,43} To explore the true origins of the red emission, another three similar R-CD samples were synthesized just by changing the amount of citric acid, i.e., 0.4, 0.8, and 1.6 g

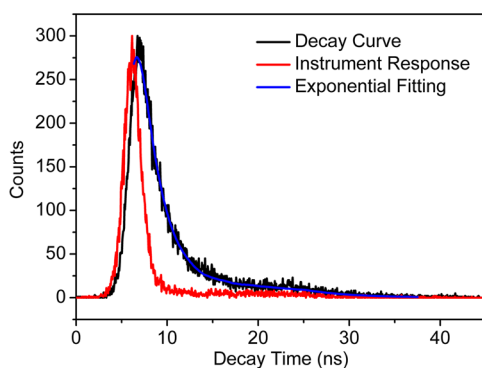


Figure 5. PL decay curve of the R-CDs measured at the emission of 627 nm under an excitation light of 560 nm.

of citric acid for synthesizing R-CDs1, R-CDs2, and R-CDs3, respectively. These R-CDs samples were analyzed and illustrated in Figures S4 and S5 as well as Tables S2 and S3. The nitrogen content of R-CD samples increases from 27.2% to 30.4% with adding the amount of citric acid, which is much higher than those of blue-emitting CDs (generally below 20%), consequently resulting in the improved light absorption and PL emission.⁴⁴ In addition, the gradual increase of the zeta potentials of the four samples indicates that more and more nitrogen atoms are doped onto R-CD surfaces (Table S4).⁴⁵ Since the incorporating N species with CDs often produce new surface states with lower energy levels,^{29,46} red fluorescence can be realized by increasing nitrogen content in CDs reasonably. To validate such a deduction, the surface states of the R-CDs, including C=O and C=N functional groups, were selectively reduced by NaBH₄.²⁹ In Figure S6, the absorption of O–H (3410 cm⁻¹) and N–H (3161 cm⁻¹) vibrations increase significantly after reduction, whereas the vibrational absorption of C=O at 1665 cm⁻¹ and C=N at 1625 cm⁻¹ decrease greatly. Meanwhile, the XPS results in Figure S7 also confirm such changes. For instance, after reduction, the C=O/C=N peak at 288.1 eV decreases in intensity whereas the peaks of C–N and C–O exhibit an increasing change. It is obvious that the variation of surface states results in the optical changes of R-CDs. In Figure 4c, the absorption spectrum of the reduced samples exhibits a significant decrease in the visible range, indicating that many surface groups like C=O and C=N were reduced.⁴⁷ Correspondingly, the maximum emission peak blue-shifts to 595 nm, as shown in Figure 4d, confirming that the surface states play a main role in modulating the PL properties of our R-CDs.^{48–50} However, the QY of the reduced R-CDs is still as high as 45% when excited with 540 nm light, which is consistent with other NaBH₄-reduced CDs.⁴⁷ Therefore, the nitrogen-derived structures in carbon cores, especially the pyrrolic N, also influence the emission efficiency of our R-CDs samples significantly.

When the R-CDs are dispersed into water, the UV–vis absorption spectra of the R-CDs display the similar absorption features to that in formamide. A slight blue-shift of 13 nm is observed in Figure S8a, which is ascribed to the increase of dielectric constant from formamide to water.¹⁵ A blue-shift of PL peak by 10 nm also occurs with the similar PL emission profiles (Figure S8b), but the QY of R-CDs drops to 24% in water, which may be ascribed to the nonradiative PL quenching induced by the newly formed hydrogen bonds between oxygen-related groups and water molecules.^{51–53} Such a phenomenon was also observed when highly luminescent CDs were

transferred from ethanol (QY = 32.5%) to water (QY = 10.8%) recently.⁵⁴ Our samples exhibit the higher QY in both solvents because the higher N doping contents of about 30% are realized in the present research. Hence, according to our present study and other researches in the literature,^{25,55} we think the nitrogen- and oxygen-related surface states and the nitrogen-derived structures in carbon cores are responsible for the strong red fluorescence of the present R-CDs.

Before biological imaging, the luminescence stability of the R-CDs aqueous solution was tested under different conditions, such as changing pH values, continuous UV irradiation, and increasing the ionic strength of the solutions (Figures S11–S14). These results confirmed the high luminescence stability of R-CDs in bioimaging environments. At first, the cytotoxicity toward HeLa cells was conducted by the standard MTT assays. The results in Figure 6 show that over 80% of HeLa cells are

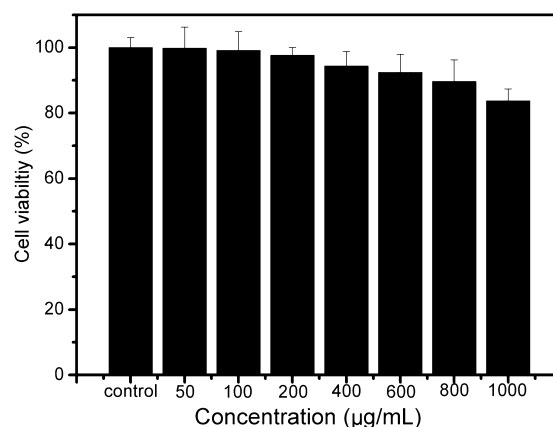


Figure 6. Viability of HeLa cells after 48 h of incubation with different concentrations of R-CDs.

still alive after incubation with 1000 µg/mL of R-CDs for 48 h, which indicates the R-CDs exhibit much lower cytotoxicity than many other inorganic nanoparticles.^{56–58} Then, 50 µg/mL of the R-CDs was incubated with the HeLa cells for different time periods (0.5–2 h), followed by observation under a confocal laser scanning microscope (CLSM). It is clear that the R-CDs gradually accumulate in the cytoplasm (Figure 7a–c) with incubation time increasing, which is a typical phenomenon of passive diffusion.⁵⁹ Meanwhile, temperature-dependent cellular uptake was also investigated to elucidate the mechanism behind the transport of carbon dots. The results in Figure 7d–f revealed that the uptake of CDs by HeLa cells accelerated as the incubation temperature increased, which indicates that the energy-dependent active endocytosis also participated in this process.⁶⁰ These results suggested that both energy-dependent endocytosis and passive diffusion involved in the cellular uptake of CDs, just like many other nanoparticles.⁶¹ Finally, the mouse imaging was also performed *in vivo*. In Figure 7h, a strong fluorescence signal at the injection site can be observed with an excitation light of 535 nm and an emission filter of 600 nm, implying that the red fluorescence of R-CDs is able to penetrate mouse skin and tissues efficiently. All these results confirm that our R-CDs can be used as an effective luminescence probe for bioimaging both *in vitro* and *in vivo*.

4. CONCLUSIONS

We have successfully prepared highly efficient red-emitting CDs on a gram scale via a facile solvothermal method and a fast

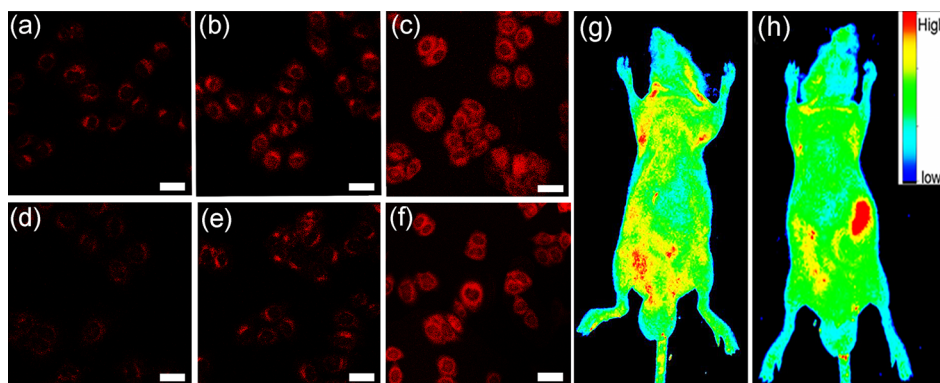


Figure 7. (a–c) CLSM images of HeLa cells incubated with 50 $\mu\text{g}/\text{mL}$ of the R-CDs for 0.5, 1, and 2 h, respectively. (d–f) CLSM images of HeLa cells incubated for 2 h at 4, 25, and 37 $^{\circ}\text{C}$, respectively. The excitation wavelength is 514 nm. PL images of a mouse (g) before and (h) after subcutaneous injection of 50 μL of the R-CDs aqueous solution (1 mg/mL). The scale bar represents 50 μm .

purification process. The as-prepared R-CDs exhibit strong absorption and emission in the visible region, high PL stability, and low cytotoxicity and thus are successfully used as a nontoxic fluorescent probe for bioimaging. In addition, detailed characterizations proved that the nitrogen- and oxygen-related surface states of R-CDs and the nitrogen-derived structures in the carbon cores are responsible for such intense red luminescence. Our present work provides a straightforward and fast approach to synthesize red emissive CDs with a high production yield, an excellent emission efficiency, and stable optical quality as well as good biocompatibility, so as to make a significant contribution to the related fields.

■ ASSOCIATED CONTENT

Supporting Information

The Supporting Information is available free of charge on the ACS Publications website at DOI: 10.1021/acs.langmuir.7b02385.

Photo image of the solid state R-CDs samples, size distribution histogram of the R-CDs, Rayleigh scattering spectra and PL spectra of both the formamide and R-CDs solution, UV–vis absorption spectra and PL spectra of the R-CDs synthesized by adding different amounts of citric acid, XPS spectra and FT-IR spectra of the NaBH_4 -reduced R-CDs, XPS spectra and FT-IR spectra of the oxidized R-CDs from refluxing in HNO_3 , the luminescence stability tests of the R-CDs aqueous solution under different conditions (PDF)

■ AUTHOR INFORMATION

Corresponding Author

*E-mail: hmxiong@fudan.edu.cn (H.-M.X.).

ORCID

Hui Ding: 0000-0002-7568-182X

Qing-Yu Gao: 0000-0002-5520-0240

Huan-Ming Xiong: 0000-0002-3118-942X

Notes

The authors declare no competing financial interest.

■ ACKNOWLEDGMENTS

This work was financially supported by the Fundamental Research Funds for the Central Universities (No. 2017QNA08), the National Natural Science Foundation of China (Grant 21771039), the Shanghai Science and Technol-

ogy Committee (No. 16DZ2270100), and China Postdoctoral Science Foundation (2016M601907).

■ REFERENCES

- (1) Baker, S. N.; Baker, G. A. Luminescent Carbon Nanodots: Emergent Nanolights. *Angew. Chem., Int. Ed.* **2010**, *49*, 6726–6744.
- (2) Lim, S. Y.; Shen, W.; Gao, Z. Carbon Quantum Dots and Their Applications. *Chem. Soc. Rev.* **2015**, *44*, 362–381.
- (3) Hu, S. Tuning Optical Properties and Photocatalytic Activities of Carbon-based “Quantum Dots” Through their Surface Groups. *Chem. Rec.* **2016**, *16*, 219–230.
- (4) Luo, P. G.; Sahu, S.; Yang, S.-T.; Sonkar, S. K.; Wang, J.; Wang, H.; LeCroy, G. E.; Cao, L.; Sun, Y.-P. Carbon “quantum” dots for optical bioimaging. *J. Mater. Chem. B* **2013**, *1*, 2116–2127.
- (5) Zhao, A.; Chen, Z.; Zhao, C.; Gao, N.; Ren, J.; Qu, X. Recent Advances in Bioapplications of C-dots. *Carbon* **2015**, *85*, 309–327.
- (6) Miao, P.; Han, K.; Tang, Y.; Wang, B.; Lin, T.; Cheng, W. Recent Advances in Carbon Nanodots: Synthesis, Properties and Biomedical Applications. *Nanoscale* **2015**, *7*, 1586–1595.
- (7) Zhu, S.; Song, Y.; Zhao, X.; Shao, J.; Zhang, J.; Yang, B. The Photoluminescence Mechanism in Carbon Dots (Graphene Quantum dots, Carbon Nanodots, and Polymer Dots): Current State and Future Perspective. *Nano Res.* **2015**, *8*, 355–381.
- (8) Pan, L.; Sun, S.; Zhang, A.; Jiang, K.; Zhang, L.; Dong, C.; Huang, Q.; Wu, A.; Lin, H. Truly Fluorescent Excitation-Dependent Carbon Dots and Their Applications in Multicolor Cellular Imaging and Multidimensional Sensing. *Adv. Mater.* **2015**, *27*, 7782–7787.
- (9) Xu, Q.; Kuang, T.; Liu, Y.; Cai, L.; Peng, X.; Sreenivasan Sreepasad, T.; Zhao, P.; Yu, Z.; Li, N. Heteroatom-doped carbon dots: synthesis, characterization, properties, photoluminescence mechanism and biological applications. *J. Mater. Chem. B* **2016**, *4*, 7204–7219.
- (10) Liu, W.; Li, C.; Ren, Y.; Sun, X.; Pan, W.; Li, Y.; Wang, J.; Wang, W. Carbon Dots: Surface Engineering and Applications. *J. Mater. Chem. B* **2016**, *4*, 5772–5788.
- (11) Zheng, M.; Ruan, S.; Liu, S.; Sun, T.; Qu, D.; Zhao, H.; Xie, Z.; Gao, H.; Jing, X.; Sun, Z. Self-Targeting Fluorescent Carbon Dots for Diagnosis of Brain Cancer Cells. *ACS Nano* **2015**, *9*, 11455–11461.
- (12) Ko, H. Y.; Chang, Y. W.; Paramasivam, G.; Jeong, M. S.; Cho, S.; Kim, S. In Vivo Imaging of Tumour Bearing Near-Infrared Fluorescence-Emitting Carbon Nanodots Derived from Tire Soot. *Chem. Commun.* **2013**, *49*, 10290–10292.
- (13) Hu, S.; Trinchì, A.; Atkin, P.; Cole, I. Tunable Photoluminescence Across the Entire Visible Spectrum from Carbon Dots Excited by White Light. *Angew. Chem., Int. Ed.* **2015**, *54*, 2970–2974.
- (14) Qu, S.; Zhou, D.; Li, D.; Ji, W.; Jing, P.; Han, D.; Liu, L.; Zeng, H.; Shen, D. Toward Efficient Orange Emissive Carbon Nanodots through Conjugated sp²-Domain Controlling and Surface Charges Engineering. *Adv. Mater.* **2016**, *28*, 3516–3521.

- (15) Sun, S.; Zhang, L.; Jiang, K.; Wu, A.; Lin, H. Toward High-Efficient Red Emissive Carbon Dots: Facile Preparation, Unique Properties, and Applications as Multifunctional Theranostic Agents. *Chem. Mater.* **2016**, *28*, 8659–8668.
- (16) Ding, H.; Yu, S. B.; Wei, J. S.; Xiong, H. M. Full-Color Light-Emitting Carbon Dots with a Surface-State-Controlled Luminescence Mechanism. *ACS Nano* **2016**, *10*, 484–491.
- (17) Dong, Y.; Pang, H.; Yang, H. B.; Guo, C.; Shao, J.; Chi, Y.; Li, C. M.; Yu, T. Carbon-Based Dots Co-doped with Nitrogen and Sulfur for High Quantum Yield and Excitation-Independent Emission. *Angew. Chem., Int. Ed.* **2013**, *52*, 7800–7804.
- (18) Liu, Z. X.; Chen, B. B.; Liu, M. L.; Zou, H. Y.; Huang, C. Z. Cu(i)-Doped carbon quantum dots with zigzag edge structures for highly efficient catalysis of azide-alkyne cycloadditions. *Green Chem.* **2017**, *19*, 1494–1498.
- (19) Tan, X.; Li, Y.; Li, X.; Zhou, S.; Fan, L.; Yang, S. Electrochemical synthesis of small-sized red fluorescent graphene quantum dots as a bioimaging platform. *Chem. Commun.* **2015**, *51*, 2544–2546.
- (20) Zhu, S.; Meng, Q.; Wang, L.; Zhang, J.; Song, Y.; Jin, H.; Zhang, K.; Sun, H.; Wang, H.; Yang, B. Highly Photoluminescent Carbon Dots for Multicolor Patterning, Sensors, and Bioimaging. *Angew. Chem., Int. Ed.* **2013**, *52*, 3953–3957.
- (21) Holzwarth, U.; Gibson, N. The Scherrer equation versus the 'Debye-Scherrer equation'. *Nat. Nanotechnol.* **2011**, *6*, 534–534.
- (22) Chua, C. K.; Sofer, Z.; Šimek, P.; Jankovský, O.; Klímová, K.; Bakardjeva, S.; Hrdličková Kučková, S.; Pumera, M. Synthesis of Strongly Fluorescent Graphene Quantum Dots by Cage-Opening Buckminsterfullerene. *ACS Nano* **2015**, *9*, 2548–2555.
- (23) Meng, X.; Chang, Q.; Xue, C.; Yang, J.; Hu, S. Full-colour carbon dots from energy-efficient synthesis to concentration-dependent photoluminescence properties. *Chem. Commun.* **2017**, *53*, 3074–3077.
- (24) Teng, X.; Ma, C.; Ge, C.; Yan, M.; Yang, J.; Zhang, Y.; Morais, P. C.; Bi, H. Green synthesis of nitrogen-doped carbon dots from konjac flour with "off-on" fluorescence by Fe³⁺ and l-lysine for bioimaging. *J. Mater. Chem. B* **2014**, *2*, 4631–4639.
- (25) Ding, H.; Wei, J. S.; Xiong, H. M. Nitrogen and Sulfur Co-doped Carbon Dots with Strong Blue Luminescence. *Nanoscale* **2014**, *6*, 13817–13823.
- (26) Pan, L.; Sun, S.; Zhang, L.; Jiang, K.; Lin, H. Near-Infrared Emissive Carbon Dots for Two-Photon Fluorescence Bioimaging. *Nanoscale* **2016**, *8*, 17350–17356.
- (27) Zhou, J.; Yang, Y.; Zhang, C. Y. A Low-Temperature Solid-phase Method to Synthesize Highly Fluorescent Carbon Nitride Dots with Tunable Emission. *Chem. Commun.* **2013**, *49*, 8605–8607.
- (28) Chen, B. B.; Li, R. S.; Liu, M. L.; Zhang, H. Z.; Huang, C. Z. Self-exothermic reaction prompted synthesis of single-layered graphene quantum dots at room temperature. *Chem. Commun.* **2017**, *53*, 4958–4961.
- (29) Nie, H.; Li, M.; Li, Q.; Liang, S.; Tan, Y.; Sheng, L.; Shi, W.; Zhang, S. X.-A. Carbon Dots with Continuously Tunable Full-Color Emission and Their Application in Ratiometric pH Sensing. *Chem. Mater.* **2014**, *26*, 3104–3112.
- (30) Zhai, Y.; Zhu, Z.; Zhu, C.; Ren, J.; Wang, E.; Dong, S. Multifunctional water-soluble luminescent carbon dots for imaging and Hg²⁺ sensing. *J. Mater. Chem. B* **2014**, *2*, 6995–6999.
- (31) Hu, S.; Chang, Q.; Lin, K.; Yang, J. Tailoring surface charge distribution of carbon dots through heteroatoms for enhanced visible-light photocatalytic activity. *Carbon* **2016**, *105*, 484–489.
- (32) Dong, X.; Su, Y.; Geng, H.; Li, Z.; Yang, C.; Li, X.; Zhang, Y. Fast one-step synthesis of N-doped carbon dots by pyrolyzing ethanolamine. *J. Mater. Chem. C* **2014**, *2*, 7477–7481.
- (33) Ding, H.; Ji, Y.; Wei, J.-S.; Gao, Q.-Y.; Zhou, Z.-Y.; Xiong, H.-M. Facile synthesis of red-emitting carbon dots from pulp-free lemon juice for bioimaging. *J. Mater. Chem. B* **2017**, *5*, 5272–5277.
- (34) Zhang, J.; Yuan, Y.; Liang, G.; Yu, S. H. Scale-Up Synthesis of Fragrant Nitrogen-Doped Carbon Dots from Bee Pollens for Bioimaging and Catalysis. *Adv. Sci.* **2015**, *2*, 1500002.
- (35) Fan, R.-J.; Sun, Q.; Zhang, L.; Zhang, Y.; Lu, A.-H. Photoluminescent carbon dots directly derived from polyethylene glycol and their application for cellular imaging. *Carbon* **2014**, *71*, 87–93.
- (36) Bao, L.; Liu, C.; Zhang, Z. L.; Pang, D. W. Photoluminescence-Tunable Carbon Nanodots: Surface-State Energy-Gap Tuning. *Adv. Mater.* **2015**, *27*, 1663–1667.
- (37) Khan, S.; Gupta, A.; Verma, N. C.; Nandi, C. K. Time-Resolved Emission Reveals Ensemble of Emissive States as the Origin of Multicolor Fluorescence in Carbon Dots. *Nano Lett.* **2015**, *15*, 8300–8305.
- (38) Qu, D.; Zheng, M.; Zhang, L.; Zhao, H.; Xie, Z.; Jing, X.; Haddad, R. E.; Fan, H.; Sun, Z. Formation Mechanism and Optimization of Highly Luminescent N-Doped Graphene Quantum Dots. *Sci. Rep.* **2015**, *4*, 5294.
- (39) Ding, H.; Xiong, H.-M. Exploring the Blue Luminescence Origin of Nitrogen-Doped Carbon Dots by Controlling the Water Amount in Synthesis. *RSC Adv.* **2015**, *5*, 66528–66533.
- (40) Jiang, K.; Sun, S.; Zhang, L.; Lu, Y.; Wu, A.; Cai, C.; Lin, H. Red, Green, and Blue Luminescence by Carbon Dots: Full-Color Emission Tuning and Multicolor Cellular Imaging. *Angew. Chem., Int. Ed.* **2015**, *54*, 5360–5363.
- (41) LeCroy, G. E.; Yang, S.-T.; Yang, F.; Liu, Y.; Fernando, K. A. S.; Bunker, C. E.; Hu, Y.; Luo, P. G.; Sun, Y.-P. Functionalized carbon nanoparticles: Syntheses and applications in optical bioimaging and energy conversion. *Coord. Chem. Rev.* **2016**, *320–321*, 66–81.
- (42) Yuan, F.; Li, S.; Fan, Z.; Meng, X.; Fan, L.; Yang, S. Shining Carbon Dots: Synthesis and Biomedical and Optoelectronic Applications. *Nano Today* **2016**, *11*, 565–586.
- (43) Hola, K.; Zhang, Y.; Wang, Y.; Giannelis, E. P.; Zboril, R.; Rogach, A. L. Carbon Dots—Emerging Light Emitters for Bioimaging, Cancer Therapy and Optoelectronics. *Nano Today* **2014**, *9*, 590–603.
- (44) Zhang, J.; Yu, S. H. Carbon dots: large-scale synthesis, sensing and bioimaging. *Mater. Today* **2016**, *19*, 382–393.
- (45) Zhang, Y.; Shen, Y.; Teng, X.; Yan, M.; Bi, H.; Morais, P. C. Mitochondria-Targeting Nanoplatform with Fluorescent Carbon Dots for Long Time Imaging and Magnetic Field-Enhanced Cellular Uptake. *ACS Appl. Mater. Interfaces* **2015**, *7*, 10201–10212.
- (46) Guo, L.; Ge, J.; Liu, W.; Niu, G.; Jia, Q.; Wang, H.; Wang, P. Tunable multicolor carbon dots prepared from well-defined polythiophene derivatives and their emission mechanism. *Nanoscale* **2016**, *8*, 729–734.
- (47) Zheng, H.; Wang, Q.; Long, Y.; Zhang, H.; Huang, X.; Zhu, R. Enhancing the Luminescence of Carbon Dots with a Reduction Pathway. *Chem. Commun.* **2011**, *47*, 10650–10652.
- (48) Bao, L.; Zhang, Z. L.; Tian, Z. Q.; Zhang, L.; Liu, C.; Lin, Y.; Qi, B.; Pang, D. W. Electrochemical Tuning of Luminescent Carbon Nanodots: From Preparation to Luminescence Mechanism. *Adv. Mater.* **2011**, *23*, 5801–5806.
- (49) Zhu, S.; Shao, J.; Song, Y.; Zhao, X.; Du, J.; Wang, L.; Wang, H.; Zhang, K.; Zhang, J.; Yang, B. Investigating the Surface State of Graphene Quantum Dots. *Nanoscale* **2015**, *7*, 7927–7933.
- (50) Song, Y.; Zhu, S.; Xiang, S.; Zhao, X.; Zhang, J.; Zhang, H.; Fu, Y.; Yang, B. Investigation into the Fluorescence Quenching Behaviors and Applications of Carbon Dots. *Nanoscale* **2014**, *6*, 4676–4682.
- (51) Yang, P.; Zhao, J.; Zhang, L.; Li, L.; Zhu, Z. Intramolecular Hydrogen Bonds Quench Photoluminescence and Enhance Photocatalytic Activity of Carbon Nanodots. *Chem. - Eur. J.* **2015**, *21*, 8561–8568.
- (52) Ghosh, D.; Ahamed, G.; Batuta, S.; Begum, N. A.; Mandal, D. Effect of an Electron-Donating Substituent at the 3',4'-position of 3-Hydroxyflavone: Photophysics in Bulk Solvents. *J. Phys. Chem. A* **2016**, *120*, 44–54.
- (53) Wang, H.; Sun, C.; Chen, X.; Zhang, Y.; Colvin, V. L.; Rice, Q.; Seo, J.; Feng, S.; Wang, S.; Yu, W. W. Excitation wavelength independent visible color emission of carbon dots. *Nanoscale* **2017**, *9*, 1909–1915.
- (54) Jiang, K.; Sun, S.; Zhang, L.; Wang, Y.; Cai, C.; Lin, H. Bright-Yellow-Emissive N-Doped Carbon Dots: Preparation, Cellular

Imaging, and Bifunctional Sensing. *ACS Appl. Mater. Interfaces* **2015**, *7*, 23231–23238.

(55) Qian, Z.; Ma, J.; Shan, X.; Feng, H.; Shao, L.; Chen, J. Highly Luminescent N-doped Carbon Quantum Dots as an Effective Multifunctional Fluorescence Sensing Platform. *Chem. - Eur. J.* **2014**, *20*, 2254–2263.

(56) Ye, D.-X.; Ma, Y.-Y.; Zhao, W.; Cao, H.-M.; Kong, J.-L.; Xiong, H.-M.; Möhwal, H. ZnO-Based Nanoplatforms for Labeling and Treatment of Mouse Tumors without Detectable Toxic Side Effects. *ACS Nano* **2016**, *10*, 4294–4300.

(57) Qian, Z.; Shan, X.; Chai, L.; Ma, J.; Chen, J.; Feng, H. Si-doped carbon quantum dots: a facile and general preparation strategy, bioimaging application, and multifunctional sensor. *ACS Appl. Mater. Interfaces* **2014**, *6*, 6797–6805.

(58) Kim, J.; Park, J.; Kim, H.; Singha, K.; Kim, W. J. Transfection and intracellular trafficking properties of carbon dot-gold nanoparticle molecular assembly conjugated with PEI-pDNA. *Biomaterials* **2013**, *34*, 7168–7180.

(59) Zhou, N.; Zhu, S.; Maharjan, S.; Hao, Z.; Song, Y.; Zhao, X.; Jiang, Y.; Yang, B.; Lu, L. Elucidating the endocytosis, intracellular trafficking, and exocytosis of carbon dots in neural cells. *RSC Adv.* **2014**, *4*, 62086–62095.

(60) Zhu, S.; Wang, L.; Zhou, N.; Zhao, X.; Song, Y.; Maharjan, S.; Zhang, J.; Lu, L.; Wang, H.; Yang, B. The crosslink enhanced emission (CEE) in non-conjugated polymer dots: from the photoluminescence mechanism to the cellular uptake mechanism and internalization. *Chem. Commun.* **2014**, *50*, 13845–13848.

(61) Lund, T.; Callaghan, M. F.; Williams, P.; Turmaine, M.; Bachmann, C.; Rademacher, T.; Roitt, I. M.; Bayford, R. The influence of ligand organization on the rate of uptake of gold nanoparticles by colorectal cancer cells. *Biomaterials* **2011**, *32*, 9776–9784.